Reports in Mechanical Engineering
Vol. 4, No. 1, 2023, pp. 175-192
ISSN: 2683-5894, DOI: https://doi.org/10.31181/rme040115092023g

Conjugate entropy generation and heat transfer of a dilute suspension of nano-encapsulated phase change material in a partially heated wall cavity

Mehdi Ghalambaz[1], Masoud Mozaffari[2], Shima Yazdani[3], Mohammad Abbaszadeh[4], Mikhail Sheremet[3], Mohammad Ghalambaz[3,*]

[1] College of Engineering, Almaaqal University, Basra 61003, Iraq
[2] Department of Mechanical Engineering, Najafabad Branch, Islamic Azad University, Najafabad 85141-43131, Iran
[3] Laboratory on Convective Heat and Mass Transfer, Tomsk State University, 634050 Tomsk, Russia
[4] Mechanical Engineering Department, Shiraz University, Shiraz, Iran

Article Info

Article history:

Received August 13, 2023
Revised September 09, 2023
Accepted September 15, 2023

Keywords:

Suspensions,
Nano-encapsulated phase change material (NEPCM),
Conjugate free convection,
Fusion temperature,
Entropy generation.

ABSTRACT

The present study offers a comprehensive simulation of conjugate heat transfer, entropy generation, and natural convection in a two-dimensional cavity filled with a water-NEPCM suspension flanked by thermally conductive solid blocks along the bottom and top walls. Utilizing weighted finite element methods on non-uniform grids, the governing equations were solved. The study varied key non-dimensional parameters like Rayleigh number (Ra), normalized block height (L_Y), and NEPCM concentration. Key findings reveal that entropy generation and Nusselt number are intricately dependent on Ra and L_Y, with the associated exponent for Ra approaching a canonical value of 1/3 as L_Y ranges from 0.05 to 0.2. Contrary to expectations, entropy generation does not invariably rise with L_Y; rather, an optimal L_Y value close to 0.2 maximizes heat transfer while minimizing entropy generation. Furthermore, increased thermal conductivity ratio (R_k) and NEPCM concentration increase the rate of heat transfer and generation of entropy. Nanoparticle fusion temperature is significant in a certain range of 0.4-0.6, containing optimal heat transfer rates.

Copyright © 2023 Regional Association for Security and crisis management and European centre for operational research. All rights reserved.

Corresponding Author:

Mohammad Ghalambaz,
Laboratory on Convective Heat and Mass Transfer, Tomsk State University, 634050 Tomsk, Russia.
Email: m.ghalambaz@gmail.com

1. Introduction

As heat and mass transfer science continues to advance, the enduring pursuit is for thermal management solutions that are both cutting-edge and efficient. A nascent but rapidly growing area in this domain is the application of NEPCMs (Nano Encapsulated Phase Change Materials) to thermal tasks. These unique materials demonstrate significant advantages, such as high-density energy storage, rapid thermal responsiveness, and regulated heat discharge characteristics (Albdour et al., 2022; Hassan et al., 2016), highly valued in various industrial, residential environments, and food applications (Alehosseini & Jafari, 2019; Ghoghaei et al., 2021).

The literature review first explores conjugate heat transfer and entropy generation in enclosures. Then, investigates some studies considering convective heat transfer of nanofluids as anno-additive enhanced

working fluids. Finally, studies related to heat transfer of NEPCM suspensions will be explored, and the contribution of the present research will be highlighted.

Studying entropy generation and heat transfer in enclosures has garnered significant attention in recent years, contributing to a more nuanced understanding of thermal management systems. Various investigations have explored different aspects of this topic, ranging from the effects of magnetic fields to the employment of nanofluids for heat transfer improvement.

The heat transfer from inside and outside of vertical hollow cylinders was explored through a comprehensive computational investigation. Different parameters were examined using a finite volume approach, including emissivity, Rayleigh numbers, and inner surface temperatures. A significant impact was found between natural convection and fluid flow characteristics by surface radiation (Chandrakar et al., 2021). Similarly, heat transfer through oriented magnetoconjugates and entropy generation in sinusoidal partitions were examined. Using a hybrid nanofluid (Ag-MgO-water), this study demonstrated the substantial effects of magnetic field intensity and cavity inclination on thermal performance and entropy generation in a hybrid nanofluid. Notably, the study established that increasing magnetic field strength reduced thermal fluid energy transfer by 11.62% while increasing cavity inclination led to 56.72% less thermal performance (Priam & Nasrin, 2021). Another study involving a thermally conductive cylinder placed centrally in a differentially heated enclosure examined the impact of heat conduction ratio with varied diameters of the cylinder. Numerical outcomes demonstrated that the thermal conductivity ratio significantly affected local heat transfer, particularly in the higher-left and lower-right corners. In higher Rayleigh numbers ($Ra=10^6$), two local circulating vortices were formed beside the cylinder, influencing heat transfer (Zhang & Su, 2021). The corrugated solid partition was also tested in a square enclosure. Air and water zones were divided by the partition, and factors such as corrugation amplitude and thermal conductivity were evaluated. A higher thermal conductivity of the partition could enhance the thermal performance by up to 25%, though the corrugation frequency seemed less significant (Priam et al., 2021).

Ishak et al. (2020) focused on the transfer of heat by convection in a trapezoidal cavity that contained a localized cylindrical solid. Their findings show that the solid cylinder's size and location serve as critical parameters in the optimization of entropy generation and heat transfer within the system. In a different setup, (Alsabery et al., 2020) evaluated the influences of a rotational cylindrical enclosure on entropy production and heat transfer. The research suggests that fluid flow and, hence, generated entropy are effectively managed by varying the rotational speed of the inner cylinder.

The impact of nanofluids on conjugate entropy generation and heat transfer in enclosures has garnered considerable attention lately, owing to its relevance in enhancing energy efficiency in both industrial and biomedical applications. The studies under consideration offer various perspectives on how nanofluids interact with various parameters to affect entropy generation and heat transfer in different enclosures. Considering free convection in nanofluids, Reddy et al. (2022) investigated natural magnetoconvection within a square enclosure saturated with a Cu/water nanofluid under a uniform magnetic field. Utilizing finite difference methods, this research reveals that increasing nanoparticle volume fractions can diminish global entropy generation. This is particularly true for systems with higher Rayleigh numbers. There is a decrease in the average Nusselt number as the magnetic field strength increases. This indicates the complex relationship between electromagnetic influence and heat transfer. Similarly, (Gowtham et al., 2022) considers the convection of aqueous nanofluids in an undulating cabinet under gravity-driven convection. The study indicates that the presence of undulations on the wavy enclosure negatively impacts global thermal performance and entropy generation rates. However, optimization is attainable when the length of the partial heater is minimized, highlighting the nuanced balance between entropy generation and heat transfer strength. (Kumar et al., 2022) ventures into the domain of mixed convection flow over a rotating disk, exploring entropy generation effects with Arrhenius activation energy. Based on their results, increasing the slip and magnetic parameters decreases fluid velocities, enhancing the generation of entropy. Besides, (Siddiqui et al., 2023) examined the utilization of ferrofluid flow within a container under non-uniform magnetic fields, focusing on radiative aspects. They found that thermal mixing and entropy generation increased as the magnetic number rose, implying a direct relationship between magnetism and thermal performance.

In an unsteady flow of nanofluids within a porous cubic container, the volume fraction of nanoparticles and Darcy number were found to be significant influences on thermal transfer and entropy generation. Thermal irreversibility notably impacted entropy generation when the Darcy number was low and fractional volumes of nanoparticles were high (Alsabery et al., 2021). An enclosure filled with TiO2-water nanofluid and its inclination angle profoundly influenced thermal performance. The heat transfer properties of pure water were shown to be superior to those of nanofluid (Tasnim et al., 2023). Using nanofluids in the annulus of a porous region, it was demonstrated that Darcy number, porosity, and nanoparticle volume fractions are significant factors influencing heat transfer. Nanofluid-porous layer heat transfer is enhanced by high Darcy number and nanoparticle volume fractions (Raizah et al., 2021). Meanwhile, the analysis of thermo-magnetic convection

showed that as the wave number grew, there was a reduction in both convection heat transfer rate and average entropy generation (Sivaraj et al., 2022). Furthermore, the influence of a heat-conducting solid fin inside a nanofluid enclosure was found to be dependent on the fin's size and position. The study showed that the optimal location of the fin could be determined by minimizing entropy generation (Le et al., 2022).

NEPCMs have the innate capability of absorbing and releasing heat, thus making them valuable in various engineering and industrial applications. Several studies have adopted computational methods, such as the high-order Galerkin finite element method, to investigate the heat transfer characteristics of NEPCM suspensions in enclosures with varying geometries and conditions. These studies collectively focus on parameters such as the Darcy parameter, fusion temperature, porosity, Stefan number, and Rayleigh number to interpret the impacts on heat transfer (Alazzam et al., 2023; Dogonchi et al., 2021; Ghalambaz et al., 2019; Hussain et al., 2022; Pasha et al., 2023). The fusion temperature has been observed to play a critical factor in the heat transfer dynamics. For instance, increasing the fusion temperature leads to a fall in flow intensity while also causing a shift in the position of the heat capacity towards the heated wall (Hussain et al., 2022). Further, fusion temperature plays an important role in optimizing the rate of heat transfer at specific values, and the optimal non-dimensional fusion temperature θ_f lies in the $0.25 < \theta_f < 0.75$ (Ghalambaz et al., 2019).

Several studies have been conducted on how the Rayleigh number and Darcy parameters affect fluid flow and heat transfer. When the Darcy parameter is increased, streamline intensity is enhanced by lowering the porous resistance, thereby boosting heat transfer in a grooved cavity (Hussain et al., 2022). Similarly, the Rayleigh number has a substantial influence, potentially significantly improving the convective heat transfer (Hussain et al., 2022; Pasha et al., 2023), with both average and local Nusselt numbers undergoing a discernible effect as Rayleigh numbers rise (Alazzam et al., 2023; Dogonchi et al., 2021).

Studies involving different geometrical configurations, such as enclosures with grooves, wavy walls, or circular cylinders, provide insights into how heat transfer patterns change under various conditions. An increase in cylinder radius or the presence of fins, for instance, can influence the phase change zones and heat transfer coefficients (Dogonchi et al., 2021; Raizah & Aly, 2021). As the Hartmann number increases, the average Nusselt number decreases, indicating that magnetic fields may moderate heat transfer (Alazzam et al., 2023). One of the standout results is that NEPCMs can enhance heat transfer rates by about 10% in comparison to the base fluid at specific fusion temperatures (Ghalambaz et al., 2019; Saleh et al., 2022). This presents a compelling case for using NEPCMs in thermal systems, providing a pathway for more energy-efficient designs.

Recent scholarly work indicates that some facets of natural convection heat transfer flows using NEPCM suspensions have been probed. However, the interconnected phenomena of entropy generation and heat transfer in these cutting-edge nanomaterials have been largely overlooked. To bridge this knowledge gap, this study scrutinizes the coupled mechanisms for entropy generation and heat transfer in NEPCM suspensions. The focal point of this investigation will be an enclosure characterized by partially heated conjugate solid walls. The aim of this research is to demonstrate how thermal and entropic phenomena are interconnected, thus enhancing the understanding of the efficacy of NEPCMs in thermal transfer applications.

2. Mathematical Framework

This study aims to assess heat transfer, conjugate natural convection, and entropy production rate within a container containing a mixture of water and dispersal NEPCM particles. This section explains the problem statement, the rest of the thermophysical properties, the governing equations, hypotheses, and boundary conditions.

2.1. Problem description

This study investigates a two-dimensional cavity geometry with two solid thermally conductive blocks attached. The cavity has heated right and left walls at temperatures T_c and T_h, while the other walls are well insulated, as shown in Figure 1. Inside the cavity is a water/NEPCMs mixture that flows through free convection.

The fusion temperature of nonadecane is approximately 32 degrees Celsius, with a latent heat of 211 kJ/kg (Barlak et al., 2016). The mixture is assumed to be homogeneous, without thermal leakage or hydrodynamic considered. The references (Barlak et al., 2016; Ghalambaz et al., 2015) are utilized to ascertain the hydrodynamic and thermal characteristics of the polyurethane (shell material), nonadecane (core material), and water (host fluid).

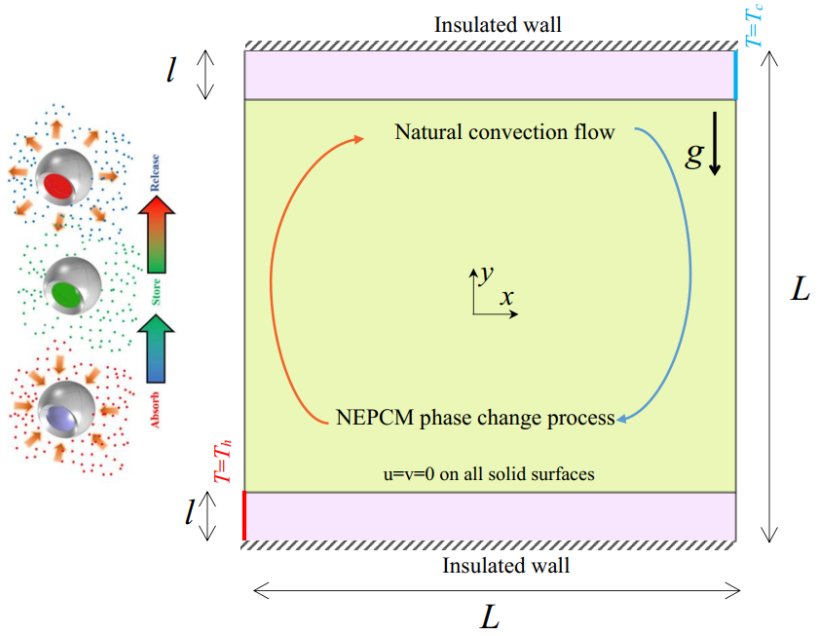

Figure 1. Visualization of boundary conditions computational domain.

2.2. Governing equations

The fundamental heat transfer equations governing the characteristics of NEPCM within the enclosure can be delineated through the principles of momentum, energy, and mass conservation, as outlined in references (Ghalambaz et al., 2019; Raizah & Aly, 2022):

$$\nabla \mathbf{u} = 0 \tag{2}$$

$$\rho_s \left(\mathbf{u}.\nabla\right)\mathbf{u} = -\nabla p + \mu_s \nabla^2 \mathbf{u} + \rho_s \beta_s \mathbf{g}\left(T - Tc\right) \tag{3}$$

$$\left(\rho C_p\right)_s \mathbf{u}.\nabla T = k_s \nabla^2 T \tag{4}$$

and for the solid wall

$$0 = k_{wall} \nabla^2 T \tag{5}$$

In this formulation, bold notations represent vector fields. Specifically, u serves as the velocity field, encompassing the y-velocity v and the x-velocity u. The scalar field for temperature is denoted by T, while the gravitational field is represented by g. Variables like dynamic viscosity μ, thermal conductivity k, density ρ, and volumetric expansion β are incorporated into the equations. The notation featuring a subscript s designates parameters specific to the NEPCM suspension. Subscripts of s and wall indicate the suspension and solid walls, respectively.

2.3. Boundary conditions

Boundary conditions involve the application of no-slip and impermeable conditions across all surfaces. Along the bottom and top solid walls of the solid walls, the temperature gradient normal to the surface, $\partial T/\partial n$, is set to zero, in which the wall normal is used (n). The sidewall portion of solid walls maintains constant temperatures of Th and Tc, as indicated in Figure 1. Moreover, at the enclosure's top-left corner, a reference pressure point is set, denoted by $p = 0$.

2.3. 1 Closure equations

For comprehensive information on the heat capacity of NEPCM particles, as well as other associated bulk properties, refer to reference (Ghalambaz et al., 2019). Calculations concerning the densities of both NEPCM suspension and NEPCM particles are detailed in (Chai et al., 2018):

$$\rho_s = \left(1-\phi\right)\rho_h + \phi\rho_{np} \tag{6a}$$

in which the subscripts of *h* an *np* denote the host fluid and nanoparticles, respectively. Then,

$$\rho_{np} = \left(\rho_{np,co}\rho_{np,shell}\right)\left(1+\iota\right)\Big/\left(\iota\rho_{np,co} + \rho_{np,shell}\right) \tag{6b}$$

in which the subscript of the *shell* indicates the nanoparticle shell, and ι=0.447 is the mass ratio of the core and the shell (Barlak et al., 2016). Besides, *co* denotes the core of the nanoparticle. The comprehensive specific heat capacity for the core of the nanoparticle, encompassing both latent and sensible heat components, is assessed according to references (Chai et al., 2018; Seyf et al., 2013):

$$Cp_{np,c} = Cp_{np,co,l} + \frac{\pi}{2}\left(\frac{h_{sf}}{\delta T} - Cp_{np,co,l}\right)\sin\left(\frac{\delta T/2 + T - T_f}{\delta T}\pi\right)\times\begin{cases}0 & T < -\delta T/2 + T_f \\ 1 & -\delta T/2 + T_f < T < \delta T/2 + T_f \\ 0 & T > \delta T/2 + T_f\end{cases} \tag{7}$$

where the subscripts *co* and *l* indicate the particle's core and liquid state. h_{sf} also denotes fusion latent heat. The nanoparticle core can undergo a phase transition at a temperature of T_f in a temperature interval of δT. The effective thermal expansion ratio, dynamic viscosity ratio, and thermal conductivity ratio for a concentration of φ can be obtained as (Chamkha et al., 2017; 2013; Zaraki et al., 2015):

$$\beta_s = \left(1-\varphi\right)\beta_h + \varphi\beta_{np} \tag{8}$$

$$\frac{\mu_s}{\mu_h} = 1 + \varphi Nv \tag{9}$$

$$\frac{k_s}{k_h} = 1 + \varphi Nc \tag{10}$$

where *Nv* and *Nc* are empirical constants for each suspension (Ghalambaz et al., 2019). Thermophysical properties of suspension samples can be found in (Barlak et al., 2016; Ghalambaz et al., 2015). The subsequent formula illustrates the entropy production process, incorporating both frictional and thermal entropy generation, as detailed in reference (Selimefendigil et al., 2016):

$$s = s_\theta + s_\psi = \frac{k_b}{T_0^{\,2}}\left[\left(\frac{\partial T}{\partial x}\right)^2 + \left(\frac{\partial T}{\partial y}\right)^2\right] + \frac{\mu_b}{T_0}\left(2\left(\left(\frac{\partial u}{\partial x}\right)^2 + \left(\frac{\partial v}{\partial y}\right)^2\right) + \left(\frac{\partial u}{\partial y} + \frac{\partial v}{\partial x}\right)^2\right) \tag{11}$$

In the equation above, the terms and correspond to entropy generation resulting from interlayer fluid friction and temperature gradients, respectively.

2.4. Scaled form control equations

For unveiling the intrinsic properties of the NEPCM suspension, a notable transformation is applied to boundary conditions and equations, leading them into a domain governed by dimensionless parameters. Consequently, a suite of non-dimensional variables emerges, orchestrating a striking and engaging transformation.

$$\left(X, Y, L_Y, \nabla\right) = \frac{\left(x, y, l, \nabla\right)}{L},\ \boldsymbol{U} = \frac{\mathbf{u}L}{\alpha_h},\ P = \frac{pL^2}{\rho_h\alpha_h^2},\ \theta = \frac{T - Tc}{Th - Tc},\ \theta_f = \frac{T_f - Tc}{\left(Th - Tc\right)} \tag{12}$$

Utilizing scaled parameters, the governing equations undergo a conversion to a dimensionless form.

$$\nabla\mathbf{U} = 0 \tag{13}$$

$$\frac{\rho_s}{\rho_h}\left(\mathbf{u}.\nabla\right)\mathbf{u} = -\nabla p + \frac{\mu_s}{\mu_h}\Pr\nabla^2\mathbf{u} + \mathrm{Ra}\Pr\theta j \tag{14}$$

$$\mathrm{Cr}\left(\mathbf{u}.\nabla\theta\right) = \frac{k_s}{k_h}\nabla^2\theta \tag{15}$$

and for the solid blocks

$$0 = R_k \nabla^2 \theta \tag{16}$$

in which the heat capacity ratio (Cr) is derived as $\varphi\lambda + \varphi\dfrac{f}{\delta\,\mathrm{Ste}} + (1-\varphi)$ (Ghalambaz et al., 2022). The scaled parameter and dimensionless numbers are:

$$Ra = \frac{g\rho_h\beta_h\Delta T L^3}{\alpha_h\mu_h},\ Pr = \frac{\mu_h}{\rho_h\alpha_h},\ \delta = \frac{\delta T}{\Delta T},\qquad R_k = \frac{k_{wall}}{k_h}$$
$$Ste = \frac{(\rho Cp)_h\,\Delta T\left(\rho_{np,shell} + \iota\rho_{np,co}\right)}{\alpha_h\left(h_{sf}\rho_{np,co}\rho_{np,shell}\right)},\ \lambda = \frac{\left(Cp_{np,co,l} + \iota Cp_{np,shell}\right)\rho_{np,core}\rho_{np,shell}}{(\rho Cp)_h\left(\rho_{np,shell} + \iota\rho_{np,co}\right)} \tag{17}$$

Besides:

$$\left(\frac{\rho_s}{\rho_h}\right) = \varphi\frac{\rho_{np}}{\rho_h} + (1-\varphi),\qquad \left(\frac{\beta_s}{\beta_h}\right) = \varphi\frac{\beta_{np}}{\beta_h} + (1-\varphi) \tag{18}$$

Moreover, it was assumed that (β_s/β_h) ~1 and (ρ_p/ρ_h)~0.74 (Barlak et al., 2016; Ghalambaz et al., 2019; Mehryan et al., 2020). Eventually, the dimensionless phase transition profile (f) is achieved as:

$$f = \frac{\pi}{2}\sin\left(\delta/2 + (\theta-\theta_f)\frac{\pi}{\delta}\right)\begin{cases} 0 & \theta < -\delta/2 + \theta_f \\ 1 & -\dfrac{\delta}{2} + \theta_f < \theta < \delta/2 + \theta_f \\ 0 & \theta > \delta/2 + \theta_f \end{cases} \tag{19}$$

The dimensionless entropy generation was also achieved as:

$$S_T = S_\theta + S_\psi = \frac{k_s}{k_h}\left[\left(\frac{\partial\theta}{\partial X}\right)^2 + \left(\frac{\partial\theta}{\partial Y}\right)^2\right] + I\frac{\mu_s}{\mu_h}\left(2\left(\frac{\partial U}{\partial X}\right)^2 + 2\left(\frac{\partial V}{\partial Y}\right)^2 + \left(\frac{\partial U}{\partial Y} + \frac{\partial V}{\partial X}\right)^2\right) \tag{20}$$

In the above equation, χ_0 serves as the irreversibility parameter and is explicitly defined by:

$$\mathrm{I} = \frac{\mu_\mathrm{h} T_0}{k_\mathrm{h}}\left(\frac{\alpha_\mathrm{h}}{\mathrm{L}(Th - Tc)}\right)^2 \tag{21}$$

The following stream function definition was also adopted for streamlining representations:

$$\nabla^2\psi = -\left(\frac{\partial V}{\partial X} - \frac{\partial U}{\partial Y}\right) \tag{22}$$

with ψ=0 at the walls. The boundary conditions were also converted as $\boldsymbol{U}$=0, θ=1, and θ=0 at the heated solid walls and $\partial\theta/\partial N$=0 at the insulated walls. The continuity of temperature and heat was also applied at the conjugate interfaces.

2.5. Total entropy generation and heat transfer rate

The overall entropy generation can be integrated over the solution domain as:

$$S = \frac{\oint_A S_T\,dA}{A} \tag{23}$$

The heat transfer rate at heated walls can be expressed as follows:

$$Nu_Y = -\frac{k_{wall}}{k_h}\left(\frac{\partial\theta}{\partial X}\right)_{@hotwall} \tag{24}$$

and the total heat transfer was defined as follows over the length of the heated wall:

$$Nu_l = \int_0^1 Nu_Y dY \tag{25}$$

3. Computational method, grid study and validation

For the numerical solution of the dimensionless governing equations and boundary conditions associated with them, the weighted finite element approach was employed, particularly the Galerkin method. A non-uniform mesh was utilized to discretize the computational domain, placing special emphasis on capturing abrupt variations in velocity and temperature near the solid boundaries through denser grid zones. The damped Newton method was chosen for solving the fully coupled discretized equations, and solutions for the ensuing linear algebraic systems were obtained via the Parallel Sparse Direct Solver. Convergence was achieved when all dependent variables' residuals reached values below 10^{-5}. For an in-depth discussion on the numerical techniques employed, one can refer to reference ("The Finite Element Method for Fluid Dynamics," 2014).

To validate the computational results, a grid sensitivity analysis was performed using five different non-uniform grid sizes. Table 1 offers an exhaustive evaluation of the temperature profiles along the vertical centerline of the enclosure for the NEPCM suspension, using relative errors benchmarked against Case 5. The investigation also furnished values for key metrics like the Nusselt number and peak velocity within the cavity, taking into account specific parameters such as R_k = 10, Ra = 10^6, L_Y=0.1, Ste = 0.3, Pr = 6.2, Nc = 6, and Nv = 3. For a more nuanced assessment, Case 3, featuring a grid of 18,000 elements, was selected, balancing both computational cost and accuracy. A view of the selected mesh is depicted in Figure 3.

Table 1. Impact of mesh elements on average Nusselt number.

Case	Sm	Elements	Nu_t	Err (%)
1	1	2000	1.952	2.6
2	2	8000	1.9803	1.2
3	3	18000	1.9925	0.6
4	4	32000	1.9995	0.2
5	5	50000	2.0039	-

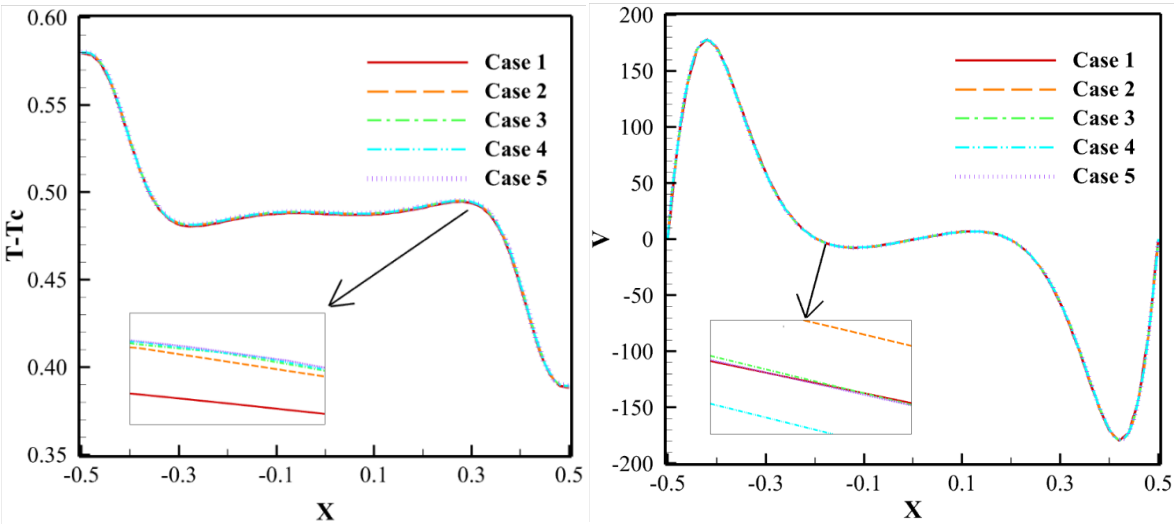

Figure 2. Temperature and *V*-velocity component along *X* coordinate at mid-plane of the enclosure at *Y*=0 for various examined meshes

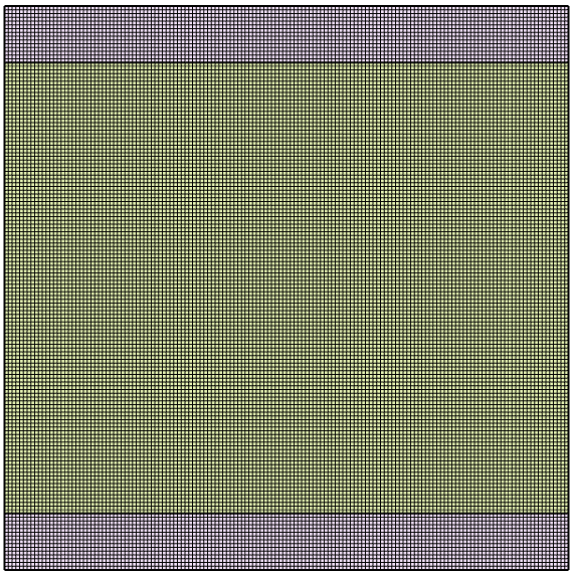

Figure 3. A view of mesh for Case 3 (*Sm*=3)

Tables 2, along with Figures 4 and 5, collectively substantiate the accuracy of the numerical code employed in this research, drawing comparisons with results detailed in references (Kahveci, 2010; Turan et al., 2011). Table 2 aligns the Nusselt numbers generated in this study against those in reference (Kahveci, 2010), which explored buoyancy-driven convection in water and TiO_2 nanoparticle suspension enclosed by thermally insulated horizontal walls and isothermally heated vertical ones. Figure 4 elucidates the variation of the Nusselt number across different nanoparticle concentration levels.

Conversely, Figure 5 conducts a meticulous examination of the temperature fields, contrasting results from our developed finite element code against data gleaned from reference (Turan et al., 2011), where a simple fluid in a square enclosure was the subject. The comparative analysis with existing literature affirms a high level of concordance, underscoring the reliability of the finite element code implemented in this study.

Table 2. Comparing the findings of the current research with Kahveci (Kahveci, 2010) (at $Ra = 10^6$).

Nu_{avg}	$\varphi = 0.0$	$\varphi = 0.05$	$\varphi = 0.1$
Kahveci (Kahveci, 2010)	9.23	9.77	10.23
Present study	9.20	9.76	10.30

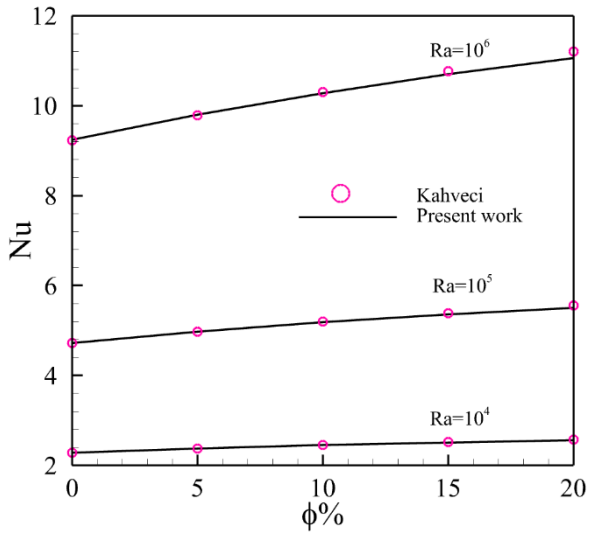

Figure 4. Comparison of Average Nusselt Numbers between the current code and data presented by Kahveci (Kahveci, 2010).

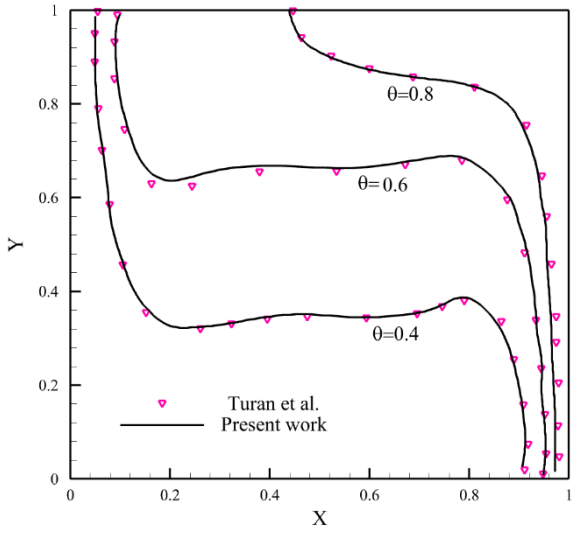

Figure 5. A comparative analysis of the temperature field between this study's numerical code and findings by Turan et al. (Turan et al., 2011) when $Ra = 10^6$.

4. Results and discussions

The study focuses on the interplay between conjugate natural convection flow and heat transfer, as well as the quantification of entropy generated as the result of the flow. The analytical setup features a container containing a fluid mixture of water and NEPCM particles. To further complicate the thermodynamics, two solid thermally conductive blocks are affixed to both the top and bottom enclosure walls.

To conduct a thorough investigation, we employ a range of non-dimensional parameters. Specifically, we vary the Rayleigh number (1e4<Ra<1e6), the normalized height of the solid blocks ($0.05<L_Y<0.2$), and the dimensionless fusion temperature ($0.1<\theta_f<0.9$). Additional parameters under consideration include the thermal conductivity ratio (R_k), ranging from 1 to 20, and NEPCM particle volume fraction (φ), varying between 0.0 and 0.05. While these parameters are varied to assess their influence, certain constants are maintained for other variables: $I=10^{-4}$, Nv = 6, Nc = 6, λ = 0.322, Pr = 6.2, δ = 0.05, Ste=0.3. The study also utilizes a default set of variable parameters, including θ_f=0.3, φ=0.05, Ra=10^6, l=0.1, and R_k=10, to serve as a baseline for comparison.

Figure 6 provides a detailed analysis of the average Nusselt number (Nu_l) and entropy generation based on Rayleigh's number (Ra) while also considering the impact of the solid block's non-dimensional height (L_Y). In conventional enclosed geometries, the Nusselt number (Nu) has a well-established relation with the Ra given

by $Nu_l = A.Ra^BPr^C$. For instance, in simple enclosures with one hot and one cold vertical wall, the exponent B usually takes a value of 1/3, as shown in MacGregor and Emer (1969) with the equation $Nu_l=0.046Ra^{1/3}$. The current analysis shows that as L_Y increases, the associated exponent for the Rayleigh number gravitates toward this canonical value. Specifically, for L_Y = 0.05, the exponent is around 0.25; for L_Y = 0.2, it is approximately 0.3. This suggests that our complex system simplifies to a uniform-temperature wall condition as L_Y increases, validating the model.

Equation (20) in the analysis points to two primary sources of entropy generation: temperature gradients and viscous forces. In this particular study, the latter can be largely discounted due to the smooth nature of the flow streamlines and minor curvature. As Ra increases, buoyancy forces augment, thereby increasing entropy generation rates primarily due to intensified temperature gradients. However, intriguingly, the rate of entropy generation does not necessarily escalate with an increase in L_Y. This behavior can be attributed to the way temperature discontinuities in the system can enhance the temperature gradient, leading, in some cases, to a reduction in entropy generation.

By juxtaposing the outcomes for Nu_l and entropy generation, it becomes evident that there exists an optimum L_Y value—likely close to 0.2—that maximizes the heat transfer coefficient without necessarily inducing the highest rate of entropy generation.

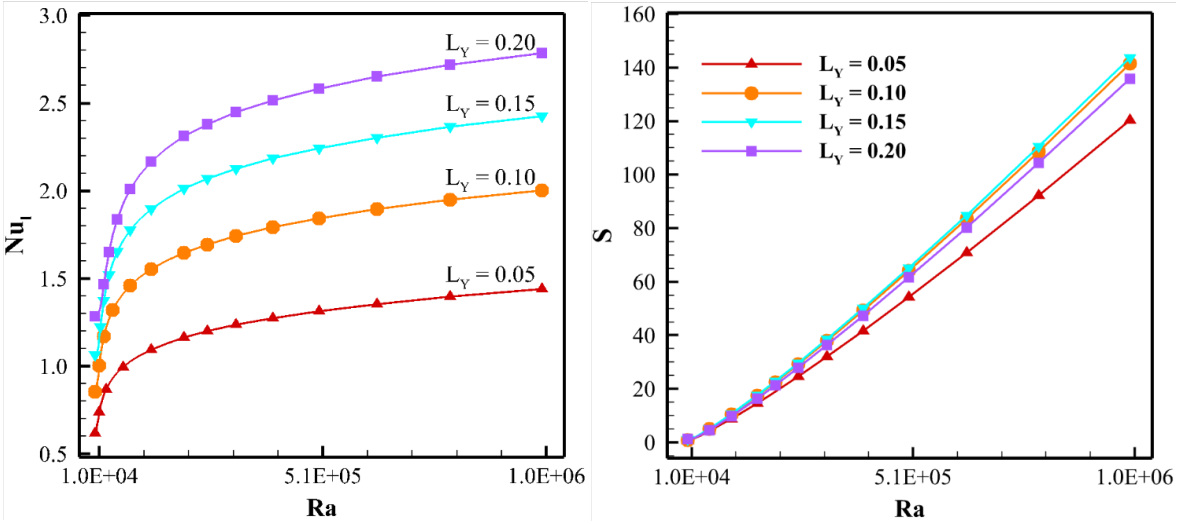

Figure 6. Plot of Rayleigh number (Ra) and varying values of the solid block's non-dimensional height (L_Y) for (a) Nusselt number average (Nu_l) and (b) entropy generation

Figure 7 presents isotherms, streamlines, and local entropy (St) for specified values of the non-dimensional height of the solid block L_Y = 0.1 and 0.2 at a fixed Rayleigh number ($Ra = 10^6$). In the left part of the figure, one observes that a rise in L_Y enhances both the heat source and sink in the system. Isotherms—lines of constant temperature—manifest around these thermal extremes. On boundaries other than those with constant temperature, these isotherms appear perpendicular to the walls, an effect of boundary insulation. Within the upper and lower regions of the solid material, a large zone of equilibrium temperature exists owing to the material's high thermal conductivity. Here, temperature variations are minimal. However, at the interface between the solid and fluid, the temperature lines exhibit an inclined orientation, indicative of a change in material conductivity.

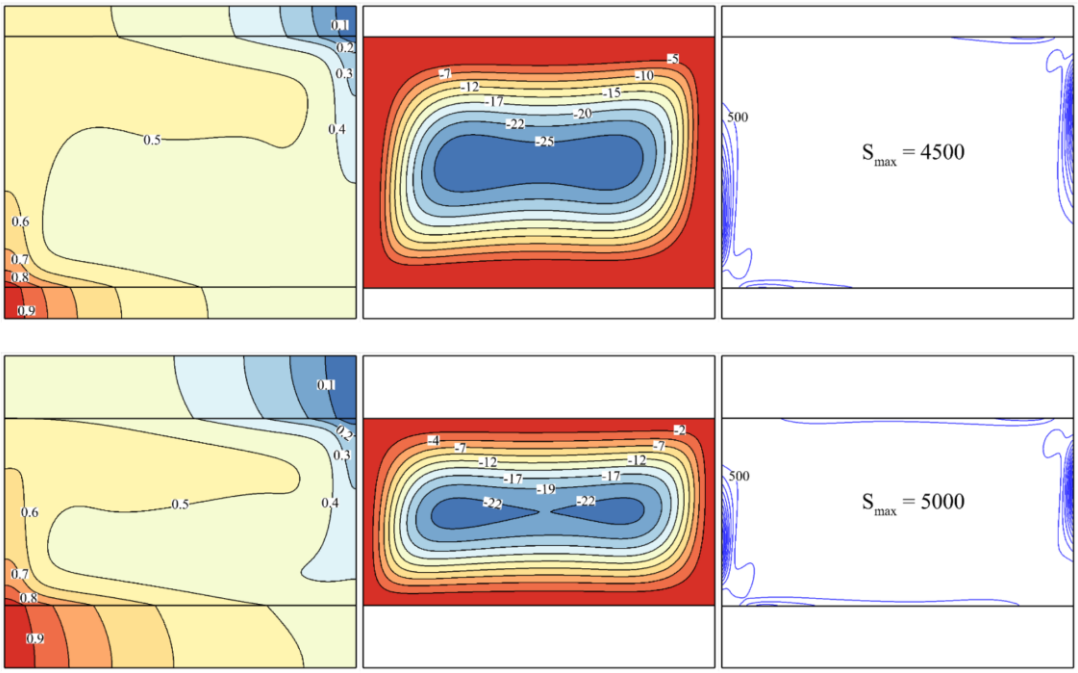

Figure 7. Isotherms, streamlines, local entropy (S_t) for selected values of L_Y (0.1 and 0.2) at Ra=10^6.

The middle section, containing the fluid, presents a distinctly different isotherm pattern compared to the regions within the solid. This is primarily due to the flow field's influence on heat distribution. Upon comparing the isotherms for L_Y = 0.1 and 0.2, it is evident that increasing L_Y leads to more closely packed temperature contours, signifying larger temperature gradients within the fluid.

The streamline patterns are presented in the central part of the figure. These streamlines delineate concentric regions influenced thermally by the lower left boundary, acting as a heat source, and the upper right boundary, functioning as a sink. These insights are vital for understanding both heat and mass transfer behavior in complex, enclosed systems.

Figure 8 displays the impact of varying the thermal conductivity ratio parameter R_k on two key metrics of the Nusselt number average Nu_l and the total entropy generation S, both plotted against the Rayleigh number Ra. In the first part of the figure focusing on the Nusselt number, one notices an exponential correlation between Nu_l and Ra for each specific value of R_k. This observation aligns with previous insights that increasing R_k at a constant L_Y exhibits behavior akin to elevating L_Y while holding R_k constant. Essentially, the impact of R_k on Nu_l follows a pattern similar to that of L_Y, reaffirming the complex but predictable relationship between these non-dimensional numbers and heat transfer efficiency.

The second part of the figure delves into total entropy generation, plotted against Ra. According to the entropy generation Eq (20), the ratio of fluid conductivity to solid conductivity does not directly influence the total entropy generated, assuming the fluid properties remain unchanged. However, an increase in R_k does signify elevated thermal conductivity for the solid. As a consequence, this leads to steeper temperature gradients within the system, thereby increasing the rate of entropy generation. This nuance underscores the intricate relationship between thermal conductivity and entropy generation rates, even when the fluid properties are kept constant.

Figure 9 delineates the isotherms, streamlines, and local entropy for selected values of the thermal conductivity ratio parameter R_k=1, 10, 20. When R_k = 1, the system essentially suffers from poor thermal conductivity as a solid block, leading to continuous temperature lines across the middle, upper, and lower regions. This continuity is expected due to the uniform material properties. Notably, the fluid's thermal conductivity is comparable to the solid wall, resulting in a much smaller heat source and sink surface at the fluid boundaries. Consequently, the buoyancy forces exerted within the fluid are weak, the streamlines display low magnitude, and the rate of entropy generation is minimized. In the limiting case where both R_k and L_Y approach zero, the temperature gradient essentially vanishes.

Conversely, an increase in R_k effectively enlarges the surface area, acting as a heat source and sink adjacent to the fluid. This expansion directly escalates the temperature gradient within the system. As a result, the generation rate of entropy correspondingly increases. This observation confirms the critical role that the ratio

of solid-to-fluid conductivity plays in modulating both the thermal gradients and the entropy generation within such complex multiphase systems.

In Figure 10, two significant trends are presented concerning the behavior of fluids containing NEPCM: (a) the variation in average Nusselt number and (b) the total entropy generation for different values of the parameters φ and θ_f. The presence of nanoparticles improves the suspension's thermal conductivity and latent heat capacity, which positively impacts the Nusselt number. Hence, as NEPCM concentration increases, so does the average Nusselt number. This is consistent with the behavior illustrated in Figure 10(a).

Moreover, the phase change region shifts closer to either the hot or cold walls of the fluid chamber as the fusion temperature of the nanoparticles increases. It is noted that at θ_f values of approximately 0.45 or 0.55, maximum heat transfer is achieved. Curiously, a local minimum in the heat transfer rate occurs at θ_f = 0.5, which, according to the study, should be avoided for optimized heat transfer. Previous studies (Zadeh et al., 2020) corroborate this behavior, highlighting that around θ_f = 0.5, NEPCMs exhibit higher efficiency in energy absorption and release mechanisms. Thus, a relative extremum in the average Nusselt number is expected around this θ_f value, as seen in Figure 10(a). In Figure 10(b), the focus shifts to the behavior of entropy generation in the system. A general trend of increasing entropy production with higher NEPCM concentration is evident. This increase aligns with Eqs. 20, which suggests that an increase in effective fluid conductivity and viscosity leads to higher entropy generation. However, a peculiar deviation is observed in the θ_f range of 0.4 to 0.6. Within this range, the rate of entropy generation decreases. This can be attributed to the fact that at θ_f = 0.5, the melting temperature of the NEPCM coincides with the average temperature of the fluid, thereby reducing the temperature gradient and, consequently, the entropy generation.

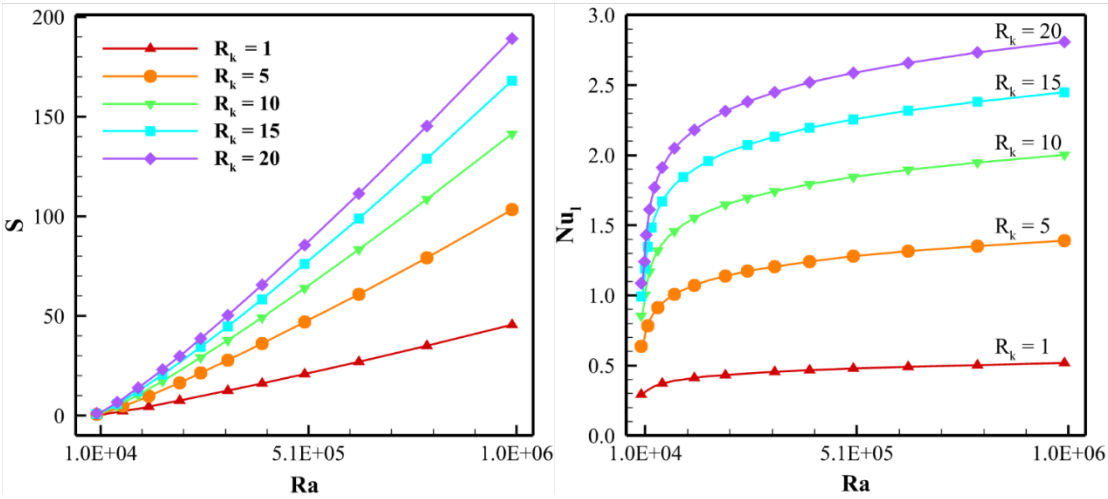

Figure 8. Plots of Ra for various values of R_k for (a) average Nusselt number and (b) total entropy generation.

Figure 11 explores the interplay between isotherms, streamlines, and local entropy (St) for a fluid containing NEPCM for specific values of θ_f = 0.1, 0.3, 0.5 at φ = 0.05. The figure reveals the sensitivity of these parameters to θ_f, indicating that the characteristics of NEPCM are closely tied to this variable. For instance, at θ_f = 0.3, the phase change occurs nearer to the cold sink, as defined by Eq. 19. This results in a less uniform temperature distribution near the cold sink and consequently higher entropy generation, particularly at the top right corner of the fluid domain. Conversely, at θ_f = 0.5, a symmetrical temperature distribution arises, mirroring the square diagonal of the fluid chamber. This symmetry is attributable to the fusion activation process being balanced between the heat source and sink. As a result, the entropy generation manifests this balance with uniform entropy production across the fluid domain.

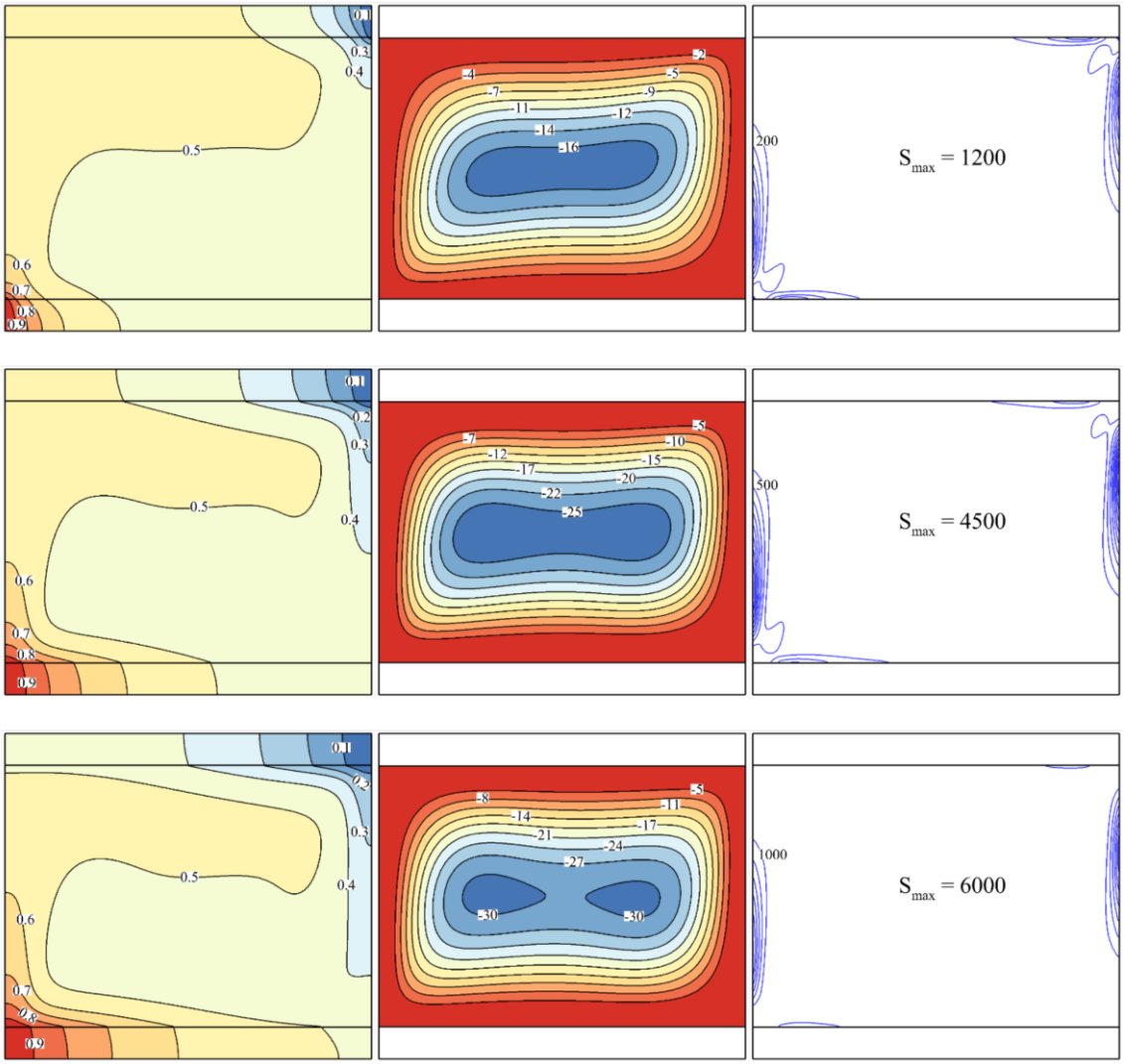

Figure 9. Isotherms, streamlines, local entropy (S_t) for selected values of R_k (1, 10, 20)

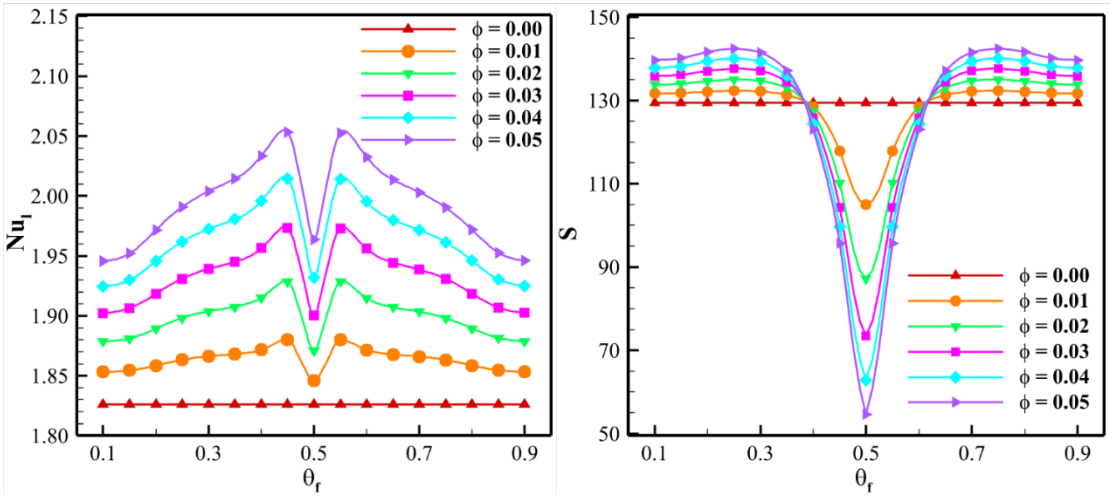

Figure 10. Plots of θ_f for various values of φ for (a) average Nusselt number and (b) total entropy generation.

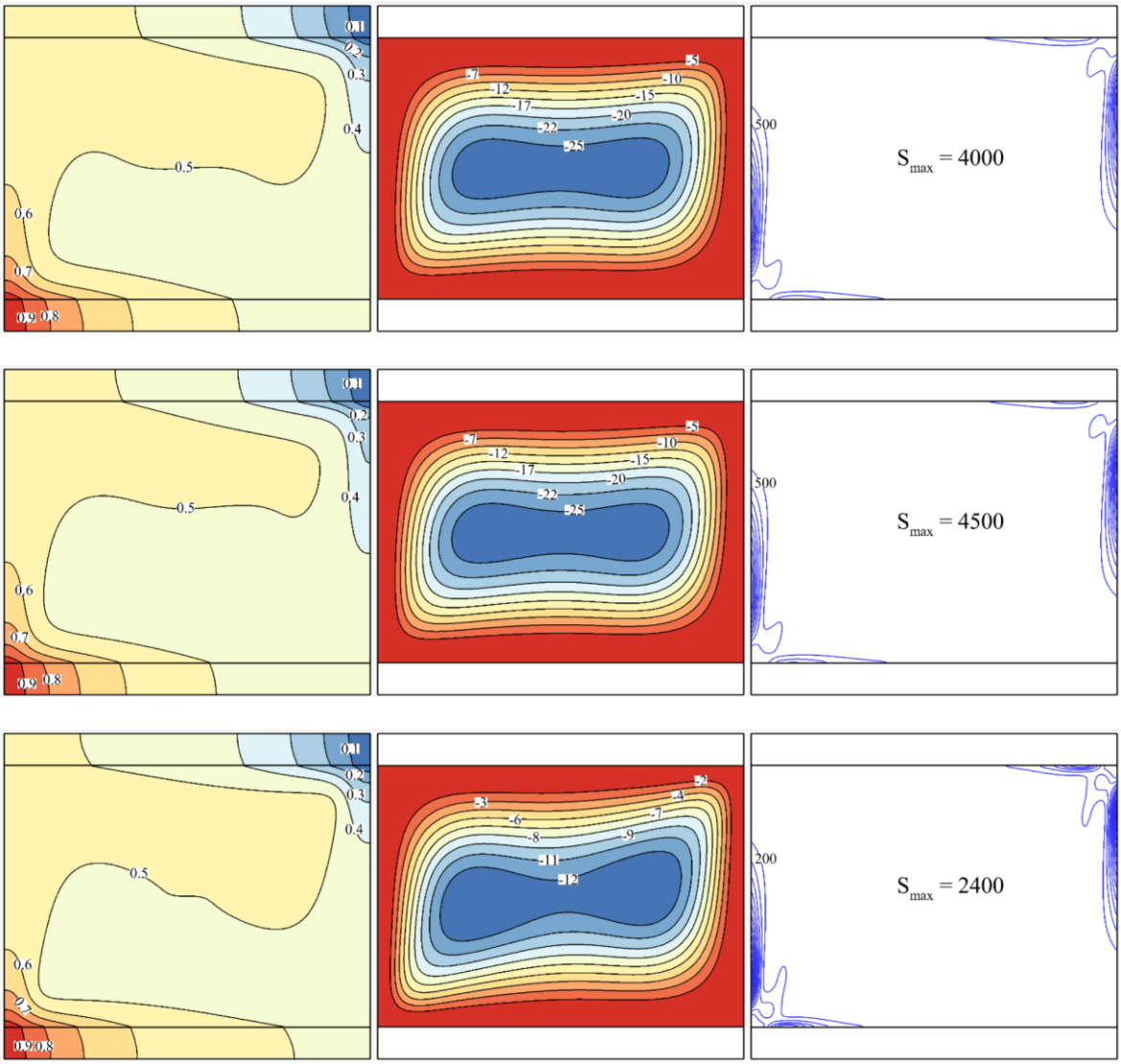

Figure 11. Isotherms, streamlines, local entropy (S_t) for selected values of θ_f (0.1, 0.3, 0.5) at φ = 0.05.

Figure 12 provides an in-depth look at the local Nusselt number in relation to various values of fusion temperature and concentrations of nanoparticles within a fluid system. The vertical axis (Y) represents the height along the heated wall, with Y=0 at the base and Y=0.1 at the top. The figure reveals that at the base of the heated wall (Y=0), the local Nusselt number is relatively low, indicating weaker conduction heat transfer. As one moves upwards along the wall toward Y=0.1, the local Nusselt number intensifies significantly. This sharp increase is attributed to the arrival of fresh cold suspension at the top of the wall, where temperature gradients reach their maximum. Consistent with earlier figures, Figure 12(a) suggests that a fusion temperature in the range of 0.4-0.6 can induce the most variability in either enhancing or deteriorating the heat transfer rate. The impact of this range on the heat transfer is also manifested in the local Nusselt number values. Additionally, an increase in nanoparticle concentration improves the heat transfer rate across the fluid system.

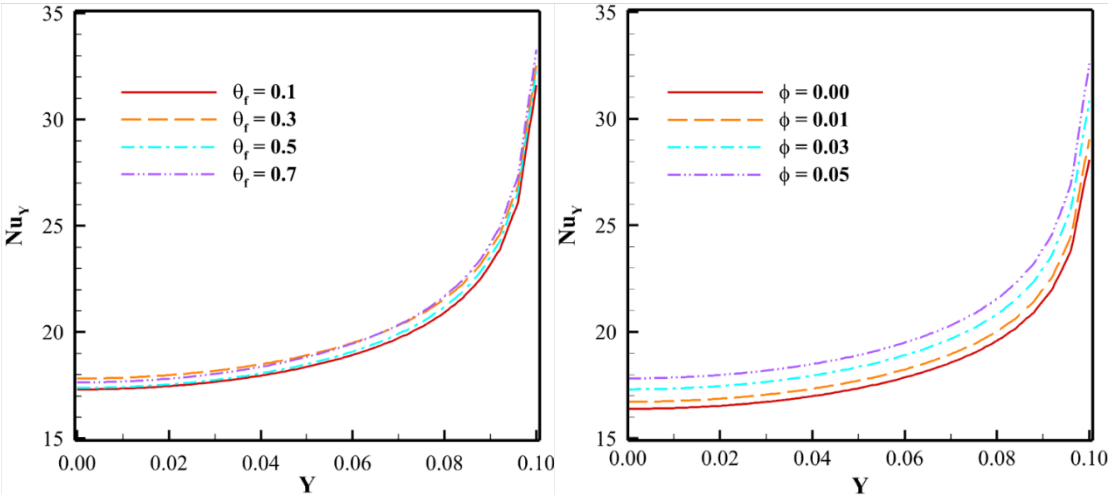

(a) (b)

Figure 12. Local Nusselt number (Nu_Y) as a function of heated solid wall length for (a) various values of θ_f and (b) various values of φ

5. Conclusions

The present article is devoted to a comprehensive investigation into the conjugate natural convection flow, heat transport, and entropy generation rate within a two-dimensional cavity filled with a suspension of water and NEPCMs. Two solid thermally conductive solid blocks were placed at the top and bottom walls. Governed by mass, momentum, and energy conservation laws, the system's behavior was numerically solved using a weighted finite element method. A non-uniform grid captured abrupt variations near the solid-fluid interface with a residual value below 10^{-5}. Various non-dimensional numbers such as Rayleigh number, normalized block height, volume concentration of NEPCM particles, and dimensionless fusion temperature of nanoparticles are varied to assess their impact. The results were reported as heat transfer (Nusselt number) and entropy generation profiles and contours. The key outcomes can be summarized as follows:

1. The average Nusselt number (Nu_l) and entropy generation are found to be strongly dependent on the Rayleigh number (Ra) and the non-dimensional height (L_Y) of the solid block. Specifically, as L_Y increases from 0.05 to 0.2, the associated exponent for Ra approaches the canonical value of 1/3, revealing that the complex system approximates a uniform-temperature wall condition.

2. Entropy generation rates are observed to primarily rise with an increase in Ra, attributed mainly to intensified temperature gradients. However, contrary to expectations, entropy generation rates do not necessarily escalate with an increase in L_Y.

3. An optimal L_Y value, estimated to be close to 0.2, is identified that maximizes the heat transfer coefficient without inducing the highest rate of entropy generation.

4. The thermal conductivity ratio (R_k) shows a complex but predictable relationship with both Nu and entropy generation. An increase in R_k results in steeper temperature gradients and, subsequently, higher rates of entropy generation.

5. Concerning NEPCM parameters, increasing the concentration (φ) positively impacts the average Nu_Y, and a peculiar behavior in entropy generation is observed in the θ_f range of 0.4 to 0.6. Here, the rate of entropy generation decreases, especially when $\theta_f = 0.5$, where the melting temperature coincides with the average fluid temperature.

6. Isotherms and streamlines reveal complex patterns that are influenced by the thermal and geometrical parameters, providing a nuanced understanding of the underlying heat and mass transfer mechanisms in the system.

References

Alazzam, A., Qasem, N. A., Aissa, A., Abid, M. S., Guedri, K., & Younis, O. (2023). Natural convection characteristics of nano-encapsulated phase change materials in a rectangular wavy enclosure with heating element and under an external magnetic field. *Journal of Energy Storage*, *57*, 106213.

Albdour, S. A., Haddad, Z., Sharaf, O. Z., Alazzam, A., & Abu-Nada, E. (2022). Micro/nano-encapsulated phase-change materials (ePCMs) for solar photothermal absorption and storage: Fundamentals, recent advances, and future directions. *Progress in Energy and Combustion Science*, *93*, 101037.

Alehosseini, E., & Jafari, S. M. (2019). Micro/nano-encapsulated phase change materials (PCMs) as emerging materials for the food industry. *Trends in Food Science & Technology*, *91*, 116-128.

Alsabery, A. I., Ismael, M. A., Chamkha, A. J., Hashim, I., & Abulkhair, H. (2021). Unsteady flow and entropy analysis of nanofluids inside cubic porous container holding inserted body and wavy bottom wall. *International Journal of Mechanical Sciences*, *193*, 106161.

Alsabery, A. I., Tayebi, T., Roslan, R., Chamkha, A. J., & Hashim, I. (2020). Entropy generation and mixed convection flow inside a wavy-walled enclosure containing a rotating solid cylinder and a heat source. *Entropy*, *22*(6), 606.

Barlak, S., Sara, O. N., Karaipekli, A., & Yapıcı, S. (2016). Thermal conductivity and viscosity of nanofluids having nanoencapsulated phase change material. *Nanoscale and Microscale Thermophysical Engineering*, *20*(2), 85-96.

Chai, L., Shaukat, R., Wang, L., & Wang, H. S. (2018). A review on heat transfer and hydrodynamic characteristics of nano/microencapsulated phase change slurry (N/MPCS) in mini/microchannel heat sinks. *Applied Thermal Engineering*, *135*, 334-349.

Chamkha, A., Doostanidezfuli, A., Izadpanahi, E., & Ghalambaz, M. (2017). Phase-change heat transfer of single/hybrid nanoparticles-enhanced phase-change materials over a heated horizontal cylinder confined in a square cavity. *Advanced Powder Technology*, *28*(2), 385-397.

Chandrakar, V., Senapati, J. R., & Mohanty, A. (2021). Conjugate heat transfer due to conduction, natural convection, and radiation from a vertical hollow cylinder with finite thickness. *Numerical Heat Transfer, Part A: Applications*, *79*(6), 463-487.

Dogonchi, A. S., Mishra, S., Karimi, N., Chamkha, A. J., & Alhumade, H. (2021). Interaction of fusion temperature on the magnetic free convection of nano-encapsulated phase change materials within two rectangular fins-equipped porous enclosure. *Journal of the Taiwan Institute of Chemical Engineers*, *124*, 327-340.

The Finite Element Method for Fluid Dynamics. (2014). In O. C. Zienkiewicz, R. L. Taylor, & P. Nithiarasu (Eds.), *The Finite Element Method for Fluid Dynamics (Seventh Edition)* (pp. iii). Butterworth-Heinemann. https://doi.org/https://doi.org/10.1016/B978-1-85617-635-4.00018-2

Ghalambaz, M., Chamkha, A. J., & Wen, D. (2019). Natural convective flow and heat transfer of nano-encapsulated phase change materials (NEPCMs) in a cavity. *International Journal of Heat and Mass Transfer*, *138*, 738-749.

Ghalambaz, M., Jin, H., Bagheri, A., Younis, O., & Wen, D. (2022). Convective Flow and Heat Transfer of Nano-Encapsulated Phase Change Material (NEPCM) Dispersions along a Vertical Surface. *Facta Universitatis, Series: Mechanical Engineering*, *20*(3), 519-538.

Ghalambaz, M., Sheremet, M. A., & Pop, I. (2015). Free convection in a parallelogrammic porous cavity filled with a nanofluid using Tiwari and Das' nanofluid model. *PloS one*, *10*(5), e0126486.

Ghoghaei, M. S., Mahmoudian, A., Mohammadi, O., Shafii, M. B., Jafari Mosleh, H., Zandieh, M., & Ahmadi, M. H. (2021). A review on the applications of micro-/nano-encapsulated phase change material slurry in heat transfer and thermal storage systems. *Journal of Thermal Analysis and Calorimetry*, *145*, 245-268.

Gowtham, S., Sivaraj, C., & Sheremet, M. A. (2022). Thermogravitational convection of water-based nanofluids with entropy generation in a wavy cabinet having a localized non-uniform heat source. *The European Physical Journal Plus*, *137*(4), 510.

Hassan, A., Shakeel Laghari, M., & Rashid, Y. (2016). Micro-encapsulated phase change materials: a review of encapsulation, safety and thermal characteristics. *Sustainability*, *8*(10), 1046.

Hussain, S., Alsedias, N., & Aly, A. M. (2022). Natural convection of a water-based suspension containing nano-encapsulated phase change material in a porous grooved cavity. *Journal of Energy Storage*, *51*, 104589.

Ishak, M. S., Alsabery, A. I., Hashim, I., & Chamkha, A. (2020). Impact of a localized solid cylinder on entropy generation and mixed convection of nanofluids in a lid-driven trapezoidal cavity. *Authorea Preprints*.

Kahveci, K. (2010). Buoyancy driven heat transfer of nanofluids in a tilted enclosure. *Journal of Heat Transfer*, *132*(6), 062501.

Kumar, A., Ray, R. K., & Sheremet, M. A. (2022). Entropy generation on double-diffusive MHD slip flow of nanofluid over a rotating disk with nonlinear mixed convection and Arrhenius activation energy. *Indian Journal of Physics*, 1-17.

Le, X. H. K., Oztop, H. F., Selimefendigil, F., & Sheremet, M. A. (2022). Entropy analysis of the thermal convection of nanosuspension within a chamber with a heat-conducting solid fin. *Entropy*, *24*(4), 523.

MacGregor, R., & Emery, A. F. (1969). Free convection through vertical plane layers—moderate and high Prandtl number fluids.

Mehryan, S., Ghalambaz, M., Gargari, L. S., Hajjar, A., & Sheremet, M. (2020). Natural convection flow of a suspension containing nano-encapsulated phase change particles in an eccentric annulus. *Journal of Energy Storage*, *28*, 101236.

Pasha, A. A., Tayebi, T., MottahirAlam, M., Irshad, K., Dogonchi, A., Chamkha, A. J., & Galal, A. M. (2023). Efficacy of exothermic reaction on the thermal-free convection in a nano-encapsulated phase change materials-loaded enclosure with circular cylinders inside. *Journal of Energy Storage*, *59*, 106522.

Priam, S. S., Ikram, M. M., Saha, S., & Saha, S. C. (2021). Conjugate natural convection in a vertically divided square enclosure by a corrugated solid partition into air and water regions. *Thermal Science and Engineering Progress*, *25*, 101036.

Priam, S. S., & Nasrin, R. (2021). Oriented magneto-conjugate heat transfer and entropy generation in an inclined domain having wavy partition. *International Communications in Heat and Mass Transfer*, *126*, 105430.

Raizah, Z., & Aly, A. M. (2021). Double-diffusive convection of a rotating circular cylinder in a porous cavity suspended by nano-encapsulated phase change materials. *Case Studies in Thermal Engineering*, *24*, 100864.

Raizah, Z., & Aly, A. M. (2022). A rotating superellipse inside a hexagonalshaped cavity suspended by nano-encapsulated phase change materials based on the ISPH method. *International Journal of Numerical Methods for Heat & Fluid Flow*, *32*(3), 956-977.

Raizah, Z. A., Alsabery, A. I., Aly, A. M., & Hashim, I. (2021). Energy and Entropy Production of Nanofluid within an Annulus Partly Saturated by a Porous Region. *Entropy*, *23*(10), 1237.

Reddy, P. B. A., Salah, T., Jakeer, S., Mansour, M., & Rashad, A. (2022). Entropy generation due to magneto-natural convection in a square enclosure with heated corners saturated porous medium using Cu/water nanofluid. *Chinese Journal of Physics*, *77*, 1863-1884.

Saleh, H., Muhandaz, R., Irma, A., Fitri, I., Fitraini, D., Sari, A., & Nufus, H. (2022). Free convection from a localized heated cylinder with nano encapsulated phase change material and water in a square enclosure. *Journal of Energy Storage*, *56*, 106028.

Selimefendigil, F., Öztop, H. F., & Chamkha, A. J. (2016). MHD mixed convection and entropy generation of nanofluid filled lid driven cavity under the influence of inclined magnetic fields imposed to its upper and lower diagonal triangular domains. *Journal of Magnetism and Magnetic Materials*, *406*, 266-281.

Seyf, H. R., Zhou, Z., Ma, H., & Zhang, Y. (2013). Three dimensional numerical study of heat-transfer enhancement by nano-encapsulated phase change material slurry in microtube heat sinks with tangential impingement. *International Journal of Heat and Mass Transfer*, *56*(1-2), 561-573.

Siddiqui, M. A., Iftikhar, B., & Javed, T. (2023). Convective heat transfer enhancement and entropy generation analysis for radiative flow of ferrofluid inside the enclosure with non-uniform magnetic field. *Journal of Magnetism and Magnetic Materials*, *584*, 171101.

Sivaraj, C., Gowtham, S., Elango, M., & Sheremet, M. (2022). Analysis of thermo-magnetic convection and entropy generation of Al2O3-water nanofluid in a partially heated wavy electronic cabinet. *International Communications in Heat and Mass Transfer*, *133*, 105955.

Tasnim, S., Mitra, A., Saha, H., Islam, M. Q., & Saha, S. (2023). MHD conjugate natural convection and entropy generation of a nanofluid filled square enclosure with multiple heat-generating elements in the presence of Joule heating. *Results in Engineering*, *17*, 100993.

Turan, O., Sachdeva, A., Chakraborty, N., & Poole, R. J. (2011). Laminar natural convection of power-law fluids in a square enclosure with differentially heated side walls subjected to constant temperatures. *Journal of Non-Newtonian Fluid Mechanics*, *166*(17), 1049-1063. https://doi.org/https://doi.org/10.1016/j.jnnfm.2011.06.003

Zadeh, S. M. H., Mehryan, S., Sheremet, M., Ghodrat, M., & Ghalambaz, M. (2020). Thermo-hydrodynamic and entropy generation analysis of a dilute aqueous suspension enhanced with nano-encapsulated phase change material. *International Journal of Mechanical Sciences*, *178*, 105609.

Zaraki, A., Ghalambaz, M., Chamkha, A. J., Ghalambaz, M., & De Rossi, D. (2015). Theoretical analysis of natural convection boundary layer heat and mass transfer of nanofluids: effects of size, shape and type of nanoparticles, type of base fluid and working temperature. *Advanced Powder Technology*, *26*(3), 935-946.

Zhang, W., & Su, X. (2021). Effect of an internal thermal-conductive cylinder on the conjugate conduction-convection in an enclosure. *Numerical Heat Transfer, Part A: Applications*, *80*(10), 505-523.